

|              |  |
|--------------|--|
| Title        | High- and Low-Energy Photoemission Study of Strongly Correlated Au-Ga-Ce Quasicrystal Approximants: Localized 4f Nature and Disorder Effects |
| Author(s)    | Nozue, Goro; Fujiwara, Hidenori; Hamamoto, Satoru et al.   |
| Citation     | Journal of the Physical Society of Japan. 2024, 93(7), p. 074703   |
| Version Type | AM   |
| URL          | <a href="https://hdl.handle.net/11094/97832">https://hdl.handle.net/11094/97832</a>  |
| rights       | ©2024 The Physical Society of Japan  |
| Note         |  |

***Osaka University Knowledge Archive : OUKA***

<https://ir.library.osaka-u.ac.jp/>

Osaka University

## High- and Low-Energy Photoemission Study of Strongly Correlated Au-Ga-Ce Quasicrystal Approximants: Localized $4f$ Nature and Disorder Effects

Goro Nozue,<sup>1,2\*</sup> Hidenori Fujiwara,<sup>1,2,3</sup> Satoru Hamamoto,<sup>1,2</sup> Akane Ose,<sup>1,2</sup> Miwa Tsutsumi,<sup>1,2</sup> Takayuki Kiss,<sup>1</sup> Atsushi Higashiya,<sup>2,4</sup> Atsushi Yamasaki,<sup>2,5</sup> Yuina Kanai-Nakata,<sup>2,6</sup> Shin Imada,<sup>2,6</sup> Masaki Oura,<sup>2</sup> Kenji Tamasaku,<sup>2</sup> Makina Yabashi,<sup>2</sup> Tetsuya Ishikawa,<sup>2</sup> Azusa Motouri,<sup>7</sup> Farid Labib,<sup>7</sup> Shintaro Suzuki,<sup>7†</sup> Ryuji Tamura,<sup>7</sup> and Akira Sekiyama<sup>1,2,3</sup>

<sup>1</sup>Division of Materials Physics, Graduate School of Engineering Science, Osaka University, Toyonaka, Osaka 560-8531, Japan

<sup>2</sup>RIKEN SPring-8 Center, Sayo, Hyogo 679-5158, Japan

<sup>3</sup>Spintronics Research Network Division, Institute for Open and Transdisciplinary Research Initiatives, Osaka University, Yamadaoka 2-1, Suita, Osaka, 565-0871, Japan

<sup>4</sup>Faculty of Science and Engineering, Setsunan University, Neyagawa, Osaka 572-8508, Japan

<sup>5</sup>Faculty of Science and Engineering, Konan University, Kobe, Hyogo 658-8501, Japan

<sup>6</sup>Department of Physical Sciences, Faculty of Science and Engineering, Ritsumeikan University, Kusatsu, Shiga 525-8577, Japan

<sup>7</sup>Department of Materials Science and Technology, Tokyo University of Science, Tokyo 125-8585, Japan

We have investigated the electronic structures of Ce-based 1/1 quasicrystal approximants  $\text{Au}_{59.2}\text{Ga}_{25.7}\text{Ce}_{15.1}$  and  $\text{Au}_{60.3}\text{Ga}_{26.1}\text{Ce}_{13.6}$  by hard X-ray photoemission (HAXPES) and high-resolution photoemission spectroscopy. The localized Ce  $4f$  electronic states are revealed for both Au-Ga-Ce approximants. Moreover, disorders in the compounds notably affect their electronic states, which has been detected by the core-level HAXPES. Valence-band photoemission spectra show the slight spectral difference depending on the composition ratio, which can be explained by a rigid-band-like shift.

### 1. Introduction

Rare-earth-based compounds with partially filled  $4f$  subshell show many intriguing quantum phenomena, such as magnetic ordering,<sup>1,2</sup> unconventional superconductivity,<sup>3,4</sup> heavy-Fermionic state<sup>5–8</sup> (rather itinerant  $4f$  electronic state with enormously enhanced effective mass), and non-Fermi-liquid behavior.<sup>9,10</sup> The strongly correlated  $4f$  electronic states in the compounds are determined by the hybridizations between the originally localized  $4f$  orbitals and itinerant conduction bands ( $c$ - $f$  hybridization), which play the important roles for these quantum phenomena. Therefore, revealing the  $4f$  electronic states is one of the fundamental issues for understanding of the mechanisms of the quantum phenomena and further developments of the functional rare-earth-based compounds.

Recently, fascinating electronic states have been reported for rare-earth-based quasicrystals (QCs) and approximants (ACs). Here, QC is a metallic alloy having an aperiodic structure with unconventional rotational symmetry forbidden to conventional crystals, and AC is a periodical metallic alloy with a similar local structure to that of QC. The unique non-Fermi-liquid behavior, which is robust against hydrostatic pressure in contrast to that in the crystalline compounds, has been observed in Au-Al-Yb QC,<sup>11</sup> whereas the superconductivity has been found in Au-Ge-Yb AC.<sup>12</sup> Moreover, ferromagnetic transition has been observed in Au-Ga-(Gd,Tb) QCs.<sup>13</sup> Consequently, the  $4f$  electronic states in QCs and

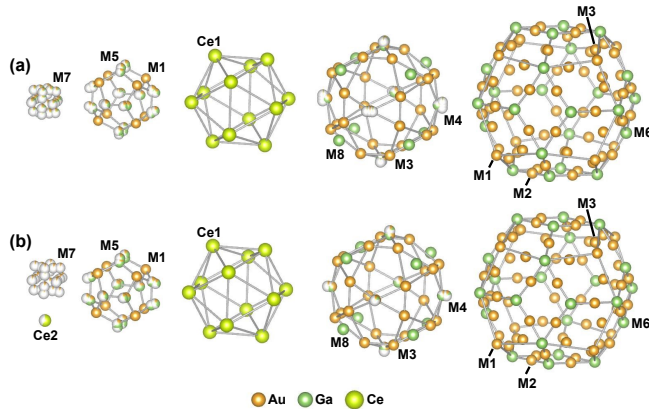


**Fig. 1.** (Color online) (a) Shell structure of the Tsai-type cluster for  $\text{Au}_{60.3}\text{Ga}_{26.1}\text{Ce}_{13.6}$  (Refs.17, 18). Chemical disorder of Au/Ga ions at the M4 and M5 sites and positional disorder due to the orientationally disordered tetrahedron at the M7 site are noticed. (b) Same as (a) but for  $\text{Au}_{59.2}\text{Ga}_{25.7}\text{Ce}_{15.1}$  in which a Ce ion occupies the cluster center (Ce2 site) with 58.1 % occupancy, in addition to the similar chemical and positional disorders observed in (a).

ACs have attracted much attention.

Conventional crystalline Ce-based compounds exhibit the characteristic electronic states as mentioned above. Thus, the physical properties of Ce-based ACs have also been investigated so far. For Ag-In-Ce,<sup>14</sup> Au-Ge-Ce,<sup>15</sup> and Au-Al-Ce ACs,<sup>16</sup> spin-glass transition has been observed. On the other hand, the presence of Kondo effect has been pointed out for

\*gnozue@decima.mp.osaka-u.ac.jp

†Present address: Department of Physics, Aoyama Gakuin University, Sagamihara, Kanagawa 258-5258, Japan

Ag-In-Ce and Au-Al-Ce ACs.<sup>14,16</sup> Meanwhile, new Ce-based Tsai-type Au-Ga-Ce 1/1 ACs have been discovered.<sup>17</sup> The Au-Ga-Ce ACs have wide range of composition ratio with single-phase region and show the spin-glass transition for all composition ratio. In  $\text{Au}_{60.3}\text{Ga}_{26.1}\text{Ce}_{13.6}$ , the Ce ions are occupied only in the icosahedron sites (Figure 1(a)).<sup>17,18</sup> On the other hand, the injection of Ce ions into the cluster center has been confirmed in  $\text{Au}_{59.2}\text{Ga}_{25.7}\text{Ce}_{15.1}$  where the Ce ions are occupied in both icosahedron sites and cluster center sites (Figure 1(b)).<sup>17,18</sup> It should be noted that the chemical disorder by non-magnetic Au/Ga atom mixing, which is indispensable for obtaining the wide range of composition ratio, would be seen in these systems. In  $(\text{Au}_{0.6975}\text{Ga}_{0.3025})_{100-y}\text{Ce}_y$ , the electrical resistivity of  $\text{Au}_{60.3}\text{Ga}_{26.1}\text{Ce}_{13.6}$  hardly depends on temperature, but slight  $-\log T$ -like temperature dependence gradually develops with increasing  $y$ .<sup>17</sup> This  $-\log T$ -like dependence is prominent for the end composition ratio  $\text{Au}_{59.2}\text{Ga}_{25.7}\text{Ce}_{15.1}$ , implying the possibility of Kondo effect in  $\text{Au}_{59.2}\text{Ga}_{25.7}\text{Ce}_{15.1}$ . In order to clarify the origins of such macroscopic properties, the element-selective electronic structure should be clarified.

To reveal the Ce  $4f$  electronic states in the Au-Ga-Ce ACs, we have performed core-level and valence-band hard X-ray photoemission spectroscopy (HAXPES). Note that HAXPES has an advantage in probing the bulk electronic states compared with conventional photoemission spectroscopy at relatively low-energy excitations.<sup>19,20</sup> We have revealed the highly localized  $4f$  electronic states in the Au-Ga-Ce ACs. Moreover, we have observed unexpected spectral broadening in the Ce  $3d$  core-level HAXPES spectra of Au-Ga-Ce ACs. From the comparison of the spectra between the Au-Ga-Ce ACs and Tsai-type AC  $\text{Cd}_6\text{Ce}$ <sup>21,22</sup> (more accurate stoichiometry composition ratio as  $\text{Cd}_{37}\text{Ce}_6$ , but hereafter denoted as  $\text{Cd}_6\text{Ce}$  for simplicity), we have revealed that the observed broadening is mainly caused by the effect of the disorders. On the other hand, it is known that a so called “pseudogap”-like structure is often seen in the density of states near the Fermi level ( $E_F$ ) for QCs and ACs.<sup>23–25</sup> We have also performed valence-band HAXPES measurement and the high-resolution photoemission spectroscopy (PES). We have observed the “pseudogap”-like structure and the composition-ratio dependence of the spectra.

## 2. Experimental details

Polycrystalline samples of Au-Ga-Ce ACs  $\text{Au}_{59.2}\text{Ga}_{25.7}\text{Ce}_{15.1}$  and  $\text{Au}_{60.3}\text{Ga}_{26.1}\text{Ce}_{13.6}$  were prepared by the arc-melting method.<sup>17</sup> The HAXPES measurements of Au-Ga-Ce ACs were performed at BL19LXU in SPring-8 with an MBS A1-HE hemispherical analyzer.<sup>26</sup> We also carried out the Ce  $3d$  core-level HAXPES of single-crystalline AC  $\text{Cd}_6\text{Ce}$  to discuss the effect of the disorders. The photon energy for HAXPES was set to 7.9 keV. The overall energy resolution was set to 500 meV for the Ce  $3d$  core-level measurements and 200 meV for the Au  $4f$  core-level and valence-band measurements. For the valence-band HAXPES of  $\text{Au}_{59.2}\text{Ga}_{25.7}\text{Ce}_{15.1}$ , we changed the linear polarization of the incident hard X-ray from the horizontal to vertical directions. The degree of linear polarization ( $P_L$ ) was estimated as  $-0.94$ , which corresponds to the linear polarization components along the horizontal and vertical directions of 3 and 97 %, respectively. The high-energy-resolution PES

measurements of Au-Ga-Ce ACs were performed using a SCIENTA SES-2002 hemispherical analyzer with an MBS T-1 discharge lamp.<sup>27,28</sup> The overall energy resolution was set to 11 meV with the Xe I resonance line (8.4 eV). The temperature was set to 7 K for HAXPES and 11 K for high-resolution PES. The clean surfaces were obtained by *in-situ* fracturing at the measuring temperatures for all measurements.

## 3. Results and discussions

### 3.1 Localized Ce $4f$ electronic states

Figure 2(a) shows the Ce  $3d$  core-level HAXPES spectra of  $\text{Au}_{59.2}\text{Ga}_{25.7}\text{Ce}_{15.1}$  and  $\text{Au}_{60.3}\text{Ga}_{26.1}\text{Ce}_{13.6}$ . Both spectra are mutually similar each other, where main peaks are seen at 884 and 902 eV in the spectra. The former (latter) is ascribed to the Ce  $3d_{5/2}$  ( $3d_{3/2}$ ) excitations, mainly corresponding to the  $3d^9 4f^1$  final states. Slight shoulder structures are seen at 878 and 896 eV, about 6 eV lower than the main peaks. These are predominantly due to the  $3d^9 4f^2$  final-states contributions, which originate from the  $c$ - $f$  hybridizations between the Ce  $4f$  orbitals and the valence bands as seen for many Ce compounds. The nearly identical spectral shape between these compounds indicates that the composition ratio dependence of  $4f$  electronic states are negligible in the Au-Ga-Ce ACs.

For comparison, the Ce  $3d$  core-level HAXPES spectra of  $\text{CeRu}_2\text{Ge}_2$  and  $\text{CeRu}_2\text{Si}_2$ <sup>29</sup> are also shown in Figure 2(a). Note that the Ce  $4f$  states in  $\text{CeRu}_2\text{Ge}_2$  are localized and magnetically ordered at low temperatures,<sup>2</sup> while  $\text{CeRu}_2\text{Si}_2$  is known as a typical heavy Fermion system with the specific heat coefficient  $\gamma \sim 350$  mJ/(K<sup>2</sup>mol) in which the  $4f$  electrons have more or less itinerant nature due to the Kondo effects.<sup>6–8</sup> The shoulder structures at 878 and 896 eV ascribed to the  $3d^9 4f^2$  final states are clearly seen in both spectra of the crystalline compounds. The  $3d^9 4f^2$  final-state contributions are definitely weaker for AC  $\text{Au}_{59.2}\text{Ga}_{25.7}\text{Ce}_{15.1}$  and  $\text{Au}_{60.3}\text{Ga}_{26.1}\text{Ce}_{13.6}$  than for  $\text{CeRu}_2\text{Ge}_2$  and  $\text{CeRu}_2\text{Si}_2$ . In addition, a small but clear peak at  $\sim 914$  eV seen in the spectrum of the heavy Fermion system  $\text{CeRu}_2\text{Si}_2$  seems to be absent in the spectra of the Au-Ga-Ce ACs as well as that of  $\text{CeRu}_2\text{Ge}_2$ . The peak at  $\sim 914$  eV is due to the  $3d^9 4f^0$  final state, which reflects the effect of itinerant behavior of the  $4f$  electrons. Instead, a broad hump structure is observed around 916 eV in the spectra of  $\text{Au}_{59.2}\text{Ga}_{25.7}\text{Ce}_{15.1}$  and  $\text{Au}_{60.3}\text{Ga}_{26.1}\text{Ce}_{13.6}$  with splitting energy of 13.3 eV from the Ce  $3d_{3/2}$  main peak. As shown in Figure 2(b), the similar hump structures are also seen in the Ga  $2p$  core-level HAXPES spectra of  $\text{Au}_{59.2}\text{Ga}_{15.7}\text{Ce}_{15.1}$  at 13.3 eV higher than the main peaks. These spectral weight are independent on element to be excited, being ascribed to the plasmon satellite. Therefore, we conclude that the  $3d^9 4f^0$  final-state contribution is absent for the Au-Ga-Ce ACs. These spectral features, the relatively weaker  $3d^9 4f^2$  contributions than even those for  $\text{CeRu}_2\text{Ge}_2$  and the negligible  $3d^9 4f^0$  spectral weight for the Au-Ga-Ce ACs, indicate that the  $4f$  electrons are highly localized in the Au-Ga-Ce ACs. Although possible itinerant  $4f$  nature due to the Kondo effect could be originally expected for  $\text{Au}_{59.2}\text{Ga}_{25.7}\text{Ce}_{15.1}$ , the localized  $4f$  electronic states in both Au-Ga-Ce ACs have been revealed by the Ce  $3d$  core-level HAXPES.

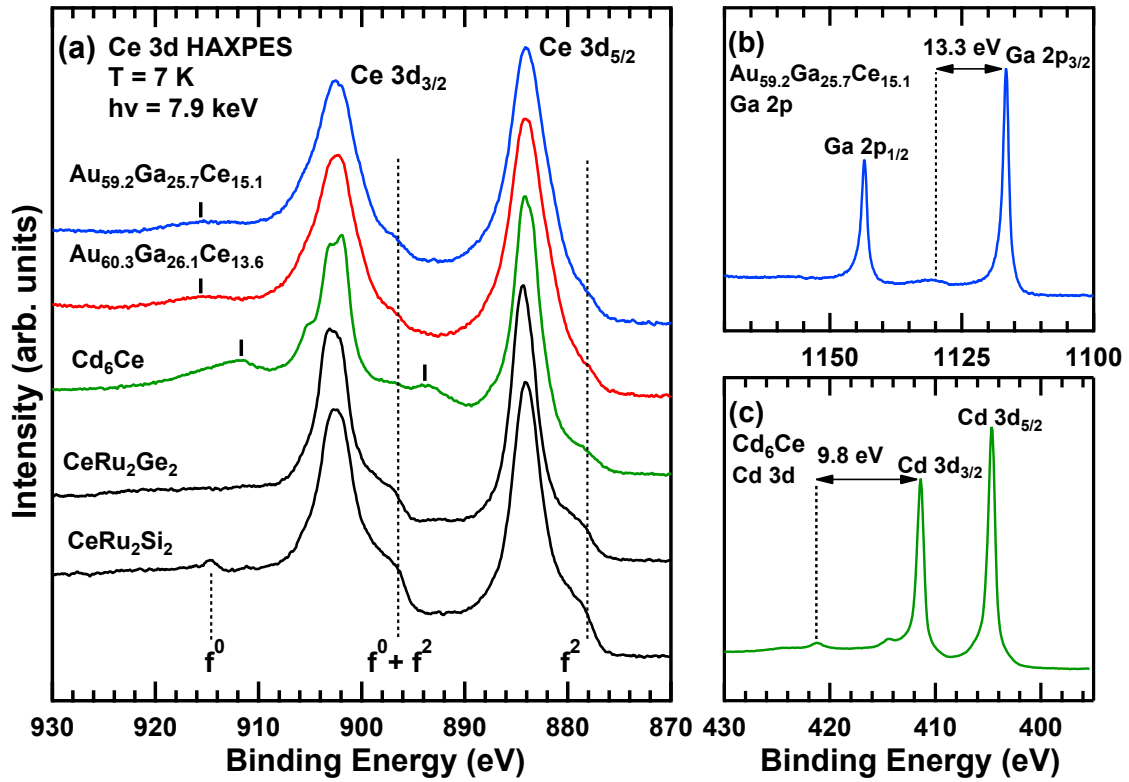


**Fig. 2.** (Color online) (a) Ce 3d core-level HAXPES spectra of  $\text{Au}_{59.2}\text{Ga}_{25.7}\text{Ce}_{15.1}$ ,  $\text{Au}_{60.3}\text{Ga}_{26.1}\text{Ce}_{13.6}$ ,  $\text{Cd}_6\text{Ce}$ ,  $\text{CeRu}_2\text{Ge}_2$ , and  $\text{CeRu}_2\text{Si}_2$ ,<sup>29)</sup> where the linear background has been subtracted from the raw spectra of  $\text{Au}_{59.2}\text{Ga}_{25.7}\text{Ce}_{15.1}$ ,  $\text{Au}_{60.3}\text{Ga}_{26.1}\text{Ce}_{13.6}$ , and  $\text{Cd}_6\text{Ce}$ . The black markers indicate the binding energies corresponding to the  $3d^94f^0$  and  $3d^94f^2$  final-state contributions. The black dashed lines indicate the plasmon satellite structures, which can be judged from the other core-level spectra of the other elements in (b) and (c). (b) Ga 2p core-level HAXPES spectrum of  $\text{Au}_{59.2}\text{Ga}_{25.7}\text{Ce}_{15.1}$ . The black dashed line shows the plasmon satellite located at the binding energy 13.3 eV higher than the Ga 2p<sub>3/2</sub> main peak. (c) Cd 3d core-level HAXPES spectrum of  $\text{Cd}_6\text{Ce}$ , in which the plasmon satellites are observed at the binding energies 9.8 eV higher than the main peaks.

### 3.2 Effect of the disorders

It is known that the two main peaks at 884 and 902 eV in the Ce 3d core-level photoemission spectra are formed by the ionic-like on-site  $3d^94f^1$  final-state multiplet structure which can become unclear when the *c-f* hybridizations become stronger.<sup>30–32)</sup> As discussed above, the 4*f* states are localized for both Au-Ga-Ce ACs. However, the  $3d^94f^1$  final-state multiplet structures seem to be smeared out in the spectra of the Au-Ga-Ce ACs. In addition, the two main peaks are much broader than those for  $\text{CeRu}_2\text{Si}_2$  and  $\text{CeRu}_2\text{Ge}_2$ . To clarify the origins of the peak broadening for the Au-Ga-Ce ACs, we have measured the Ce 3d core-level HAXPES spectrum of Tsai-type AC  $\text{Cd}_6\text{Ce}$  with no chemical and almost negligible positional disorders,<sup>21,22)</sup> as shown in Figure 2(a). The clear  $3d^94f^1$  multiplet structures are seen in the Ce 3d main peaks (clearer in the  $3d_{3/2}$  peaks centered at 902 eV) for AC  $\text{Cd}_6\text{Ce}$ . The Ce 4*f* electronic states are found to be localized also for AC  $\text{Cd}_6\text{Ce}$ , of which the  $3d^94f^2$  final-state spectral weight is weaker than that for  $\text{CeRu}_2\text{Ge}_2$  and the  $3d^94f^0$  peaks are negligible. Broad peaks centered at 894 and 912 eV in the Ce 3d core-level spectra of AC  $\text{Cd}_6\text{Ce}$ , being 9.8 eV higher than the main  $3d^94f^1$  peaks, are ascribed to the plasmon excitations which are also observed in the Cd 3d core-level spectrum as shown in Figure 2(c). From our finding about the localized nature of the 4*f* states for all ACs surveyed here and the fact that the chemical and positional disorders (their details are explained later) are seen for the Au-Ga-Ce ACs in contrast to AC  $\text{Cd}_6\text{Ce}$ ,<sup>21,22)</sup> we conclude

that the remarkable broadening of the Ce 3d core-level photoemission spectra of the Au-Ga-Ce ACs originates (at least, partly) from the disorders. Note that the Ce 3d main peaks of Au-Ga-Ce ACs are also broader than those of polycrystalline CePdSn with localized Ce 4*f* system,<sup>33)</sup> where the multiplet structures are seen in the Ce  $3d_{3/2}$  peak for CePdSn.<sup>34)</sup> Thus, the peak broadening seen for the Au-Ga-Ce ACs is not simply explained by the effect of their polycrystalline structures.

We focus on the two main peaks in the Ce 3d spectra of Au-Ga-Ce ACs and AC  $\text{Cd}_6\text{Ce}$  corresponding to the  $3d^94f^1$  contributions. Figure 3(a) shows the Ce  $3d_{3/2}$  and Ce  $3d_{5/2}$  peaks of Au-Ga-Ce ACs and AC  $\text{Cd}_6\text{Ce}$ . In AC  $\text{Cd}_6\text{Ce}$ , the  $3d^94f^1$  final-state multiplet structures are clearly observed as mentioned above. In order to estimate how much the Ce 3d core-level HAXPES spectra of the Au-Ga-Ce ACs are broadened beyond the life-time and instrumental broadenings, we have broadened the Ce 3d spectrum of AC  $\text{Cd}_6\text{Ce}$  to roughly fit the spectra of the Au-Ga-Ce ACs. Figure 3(b) shows the comparison of the spectra after the broadening by the Gaussian with the full width at half maximum (FWHM) of 2.2 eV for the spectrum of AC  $\text{Cd}_6\text{Ce}$ . This value is much larger than that of the instrumental broadening of 0.5 eV, reflecting the effect of the disorders in the Au-Ga-Ce ACs as well as their polycrystalline structures. In order to further reveal the effect on the other sites, we have measured the Au 4*f* core-level HAXPES spectra of  $\text{Au}_{59.2}\text{Ga}_{25.7}\text{Ce}_{15.1}$  and the Au metal evaporated on the sample surface, as shown in Figure 3(c). The Au 4*f* peaks of  $\text{Au}_{59.2}\text{Ga}_{25.7}\text{Ce}_{15.1}$  are shifted by

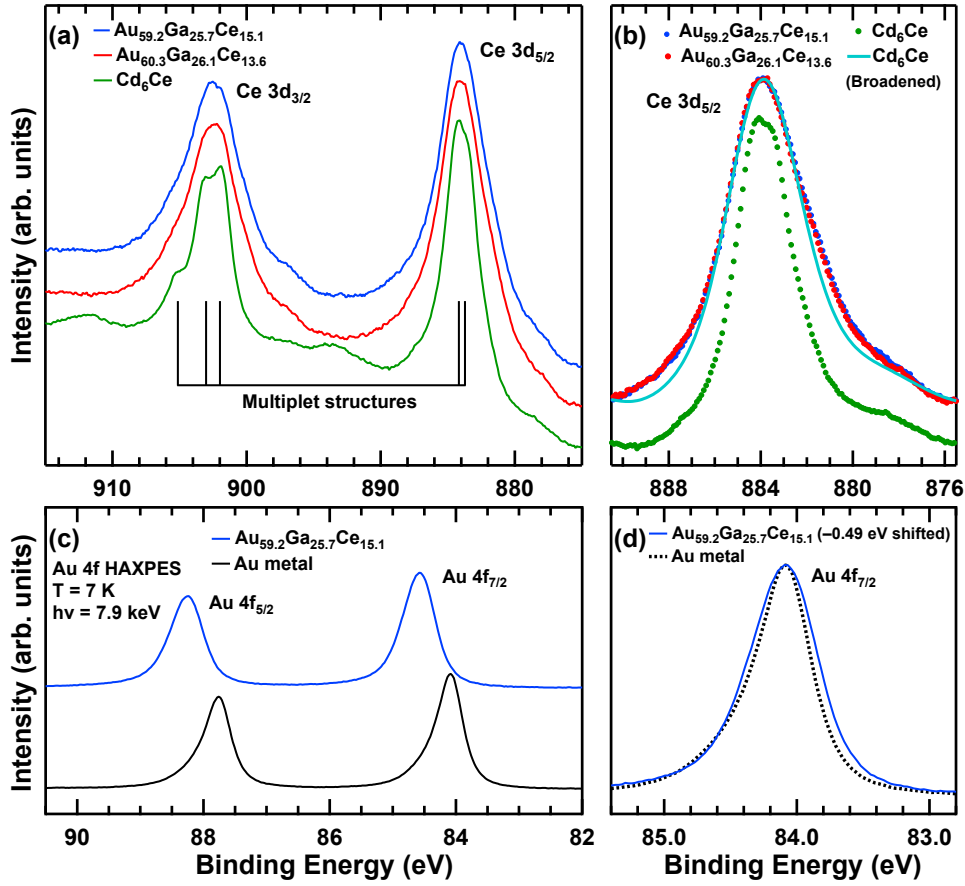


**Fig. 3.** (Color online) (a) Enlarged view of the Ce  $3d$  core-level photoemission spectra of AC  $\text{Au}_{59.2}\text{Ga}_{25.7}\text{Ce}_{15.1}$ ,  $\text{Au}_{60.3}\text{Ga}_{26.1}\text{Ce}_{13.6}$ , and  $\text{Cd}_6\text{Ce}$  focused on the main peaks. The vertical black lines indicate the  $3d^94f^1$  final-state multiplet components for  $\text{Cd}_6\text{Ce}$ . (b) Comparison of the Ce  $3d_{5/2}$  main peaks after subtracting the Shirley-type backgrounds among the ACs. For  $\text{Cd}_6\text{Ce}$ , broadened spectra by a Gaussian with the full width at half maximum of 2.2 eV to roughly fit the widths of the spectra of the Au-Ga-Ce ACs. (c) Au  $4f$  core-level HAXPES spectra of  $\text{Au}_{59.2}\text{Ga}_{25.7}\text{Ce}_{15.1}$  and Au metal. (d) Comparison of the Au  $4f_{7/2}$  HAXPES spectra between AC  $\text{Au}_{59.2}\text{Ga}_{25.7}\text{Ce}_{15.1}$  and Au metal where the spectrum of  $\text{Au}_{59.2}\text{Ga}_{25.7}\text{Ce}_{15.1}$  is shifted by  $-0.49$  eV.

0.49 eV to higher binding energy relative to those of the polycrystalline Au metal. To discuss the difference of the peak width, the Au  $4f$  spectrum of  $\text{Au}_{59.2}\text{Ga}_{25.7}\text{Ce}_{15.1}$  is shifted by  $-0.49$  eV and compared with that of the Au metal as shown in Figure 3(d). We have confirmed that the Au  $4f$  peaks of  $\text{Au}_{59.2}\text{Ga}_{25.7}\text{Ce}_{15.1}$  is broader than that of the Au metal as seen in the comparison of the Ce  $3d$  spectra between the Au-Ga-Ce and Cd-Ce ACs. However, the broadening of the Ce  $3d$  peaks is larger than that of the Au  $4f$  peaks in  $\text{Au}_{59.2}\text{Ga}_{25.7}\text{Ce}_{15.1}$  for which the broadening with FWHM of 0.24 eV (not shown in the figure) has been estimated. These results indicate that the disorders affect the overall electronic states of the Au-Ga-Ce ACs although the effect on the Au sites is relatively smaller than that on the Ce sites.

The core-level peak broadening observed for the Ce and Au sites is ascribed to inhomogeneity of the core-level energy depending on site. Namely, the binding energy on each site would be deviated from the mean binding energy. Since the observed core-level photoemission spectra are formed by the superposition of the spectra from all sites, the deviation of the binding energy reflects the broadening effects. In general, the shift of the core-level binding energy  $\Delta E$  can be given by the following formula:<sup>35)</sup>

$$\Delta E = \Delta\mu + K\Delta Q + \Delta V_M - \Delta E_R \quad (1)$$

where  $\Delta\mu$  denotes the change in the chemical potential,  $K$  and  $\Delta Q$  stand for the Coulomb coupling constant between the valence and core electrons, and the change in the number of valence electrons on the atom considered, respectively,  $\Delta V_M$  represents the change in Madelung potential, and  $\Delta E_R$  denotes the change in the extra-atomic relaxation energy which is important for metallic atoms/ions.<sup>36)</sup> It should be noted that the effect of the polycrystalline structure is not included in Eq. (1). The first term  $\Delta\mu$  can be ruled out from the origins of the shift leading to the broadening since we discuss the site dependence within the same compound. The positional and chemical disorders have been observed on M4, M5, and M7 sites of the Au-Ga-Ce ACs (Figure 1).<sup>17)</sup> From these disorders, the local environment and Madelung potential are different at each Ce site in the Au-Ga-Ce ACs. It should be noted that the mutually similar Ce  $3d$  core-level HAXPES spectra of Au-Ga-Ce ACs indicate that the effect of Ce injection into the icosahedron sites is minor compared with the effect of the other disorders or this effect is too small to detect within our experimental conditions. Meanwhile, the effects of the second and fourth terms ( $K\Delta Q$  and  $\Delta E_R$ ) would be minor in the Ce  $3d$  spectra, which is concluded from the comparison of the spectra with that of AC  $\text{Cd}_6\text{Ce}$  where the Ce  $4f$  states are found to be localized with the  $\text{Ce}^{3+}$  configuration in all Ce-based ACs discussed above. Therefore, we can conclude that the broad-

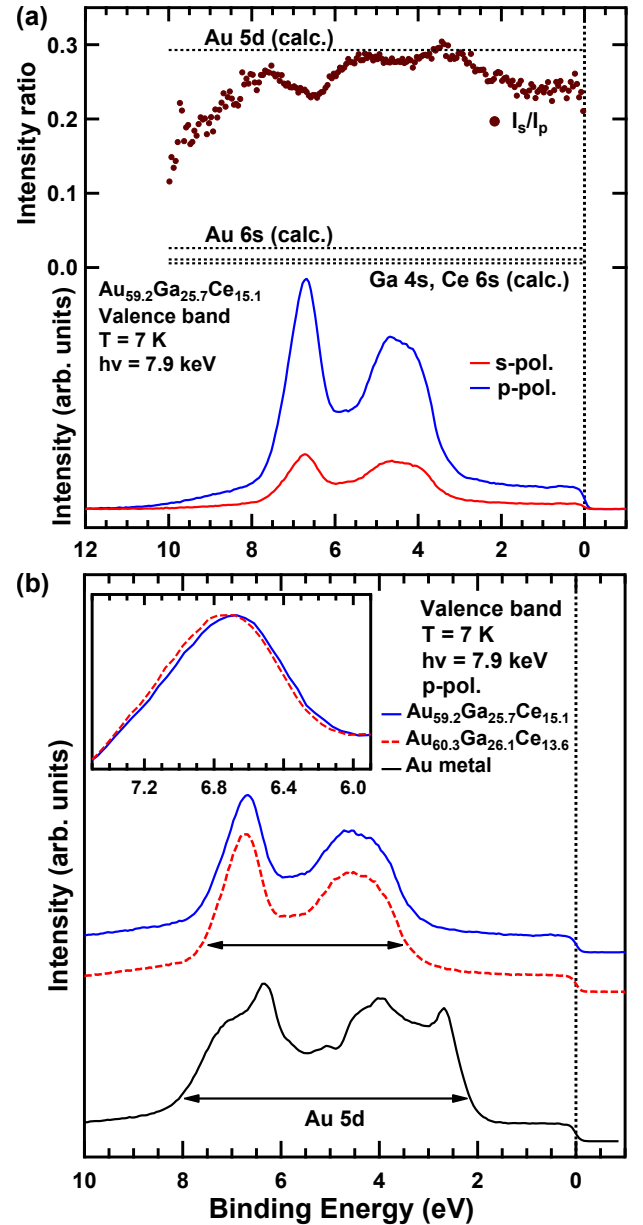
ening of the Ce 3*d* core-level photoemission spectra by the disorders is ascribed to  $\Delta V_M$ . On the other hand, the relatively less broadening of the Au 4*f* core-level spectra (FWHM of 0.24 eV) would be due to a compensation by the extra-atomic relaxation ( $\Delta E_R$ ) yielded by the screening of the conduction electrons in the Au sites.

### 3.3 Valence-band photoemission spectroscopy

The polarization-dependent valence-band HAXPES is useful to reveal the orbital contribution in the valence-band electronic states.<sup>37)</sup> Figure 4(a) shows the polarization-dependent valence-band HAXPES spectra of  $\text{Au}_{59.2}\text{Ga}_{25.7}\text{Ce}_{15.1}$ . In both *p*- and *s*-polarization configurations, prominent spectral weights are observed in the binding energy region between 3 and 8 eV. In order to estimate the orbital contributions for this structure, the photoelectron intensity ratio ( $I_s/I_p$ ) for the *s*-polarization ( $I_s$ ) to the *p*-polarization ( $I_p$ ) is also shown in Figure 4(a) whereas the calculated  $I_s/I_p$  values and photoionization cross-sections (relative to those for the Au 5*d* orbitals) for the orbitals forming the valence bands are listed in Table 1.<sup>38–41)</sup> The experimental  $I_s/I_p$  closes to the calculated Au 5*d* value of  $I_s/I_p$  between 3 and 8 eV. This result as well as the fact that the Au 5*d* contribution is much predominant at the photoelectron kinetic energy ( $h\nu$ ) of  $\sim 8$  keV means that the pronounced structures between 3 and 8 eV originate from the Au 5*d* bands. Moreover, the experimental  $I_s/I_p$  in the vicinity of  $E_F$  is much larger than calculated value for *s* orbitals and comparable to that found in the Au metal,<sup>37)</sup> which indicates that the Au 5*d* orbital contributes to the density of states even around  $E_F$ .

Figure 4(b) shows the valence-band HAXPES spectra of  $\text{Au}_{59.2}\text{Ga}_{25.7}\text{Ce}_{15.1}$  and  $\text{Au}_{60.3}\text{Ga}_{26.1}\text{Ce}_{13.6}$  in the *p*-polarization configuration, which are compared with the HAXPES spectrum of the Au metal evaporated on the sample surface where the evaporated Au layer is much thicker than the photoelectron probing depth. The spectral shape of both Au-Ga-Ce ACs is mutually similar including the pronounced structures between 3 and 8 eV. Therefore, the Au 5*d* contributions are also dominant in the valence-band HAXPES spectrum of  $\text{Au}_{60.3}\text{Ga}_{26.1}\text{Ce}_{13.6}$ . The observed main Au 5*d* bands between 3 and 8 eV in the Au-Ga-Ce ACs are narrower than those of the Au metal where the top of the main Au 5*d* bands is located at  $\sim 2$  eV. Actually, the surface color of the ACs is silver-like, which is consistent with the spectral feature with the top of the 5*d* valence bands are located at  $\sim 3$  eV as shown in Fig. 4(b). A slight difference depending on the composition ratio is observed in the valence-band HAXPES spectra. The inset of Fig. 4(b) shows an enlarged view of the spectra around the pronounced structures in 7 eV for  $\text{Au}_{59.2}\text{Ga}_{25.7}\text{Ce}_{15.1}$  and  $\text{Au}_{60.3}\text{Ga}_{26.1}\text{Ce}_{13.6}$ . The structure of  $\text{Au}_{60.3}\text{Ga}_{26.1}\text{Ce}_{13.6}$  is shifted by about 60 meV to higher binding energy relative to that of  $\text{Au}_{59.2}\text{Ga}_{25.7}\text{Ce}_{15.1}$ . The similar slight shift is also observed around 4 eV (not shown in the figure).

To further investigate the composition-ratio dependence of the electronic structure, we have performed the high-resolution PES at  $h\nu = 8.4$  eV. Figure 5(a) shows the high-resolution PES spectra of  $\text{Au}_{59.2}\text{Ga}_{25.7}\text{Ce}_{15.1}$  and  $\text{Au}_{60.3}\text{Ga}_{26.1}\text{Ce}_{13.6}$  near  $E_F$ . In both spectra, a slight reduction of the spectral weight toward  $E_F$  is observed whereas no peak structure is found. These reductions are reported as the

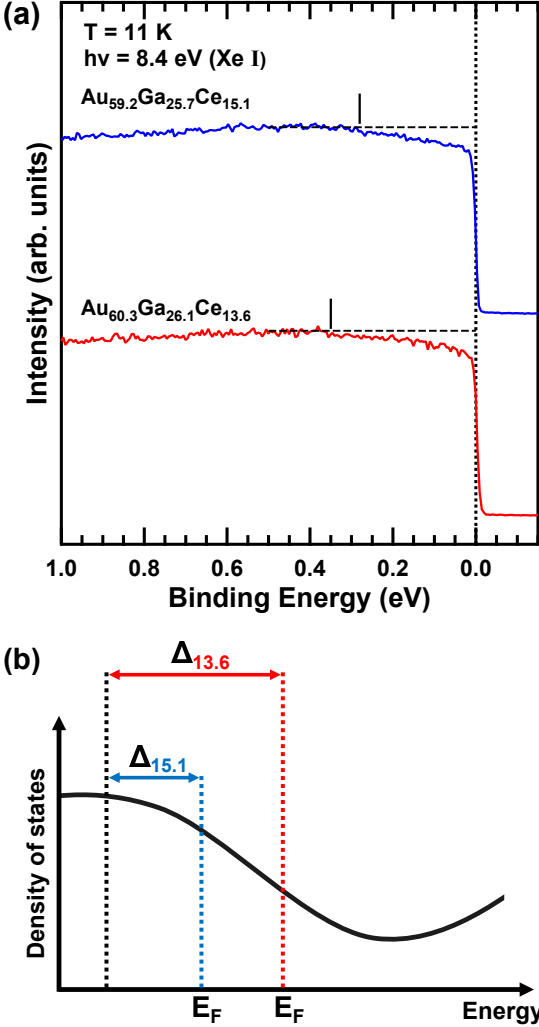


**Fig. 4.** (Color online) (a) Linear polarization dependence of the valence-band HAXPES spectra (bottom) and the photoelectron intensity ratio  $I_s/I_p$  (top) of  $\text{Au}_{59.2}\text{Ga}_{25.7}\text{Ce}_{15.1}$  after subtracting the Shirley-type backgrounds. The spectral weights at different polarization configurations have been normalized by the photon flux. (b) Valence-band HAXPES spectra of  $\text{Au}_{59.2}\text{Ga}_{25.7}\text{Ce}_{15.1}$ ,  $\text{Au}_{60.3}\text{Ga}_{26.1}\text{Ce}_{13.6}$ , and Au metal in the *p*-polarization configuration. The inset shows the enlarged view of the spectra around 7 eV.

“pseudogap” in the previous PES studies.<sup>23–25)</sup> The slightness of the reduction at  $E_F$  compared with that for the other ACs and QCs<sup>23–25)</sup> could be caused by the disorders observed for the Au-Ga-Ce ACs when the spectral reduction at  $E_F$  is assumed to be intrinsic for QCs and ACs with less disorders. Meanwhile, the binding energy at which the spectral intensity starts to decrease is slightly different between the compounds. The spectral weight starts to decrease (toward  $E_F$ ) at the binding energy of  $0.28 \pm 0.03$  eV in  $\text{Au}_{59.2}\text{Ga}_{25.7}\text{Ce}_{15.1}$ , which is defined here as  $\Delta_{15.1}$  and has been estimated from the differential of the smoothed spectrum (not shown here). For  $\text{Au}_{60.1}\text{Ga}_{26.1}\text{Ce}_{13.6}$ , the binding energy  $\Delta_{13.6}$  at which the intensity starts to decrease has been obtained as  $0.35 \pm 0.03$  eV.

**Table I.** Calculated photoelectron intensity ratio  $I_s/I_p$  and relative photoionization cross sections per electron  $\sigma$  for Au  $5d$ , Au  $6s$ , Ga  $4s$ , Ga  $4p$ , Ce  $4f$ , and Ce  $6s$  orbitals at the kinetic energy of 8 keV.<sup>38–41)</sup>

| Orbital   | Au $5d$ | Au $6s$ | Ga $4s$ | Ga $4p$ | Ce $4f$ | Ce $6s$ |
|-----------|---------|---------|---------|---------|---------|---------|
| $I_s/I_p$ | 0.293   | 0.026   | 0.011   | 0.469   | 0.853   | 0.006   |
| $\sigma$  | 1       | 0.39    | 0.43    | 0.06    | 0.03    | 0.16    |

**Fig. 5.** (Color online) (a) High-resolution valence-band PES spectra of  $\text{Au}_{59.2}\text{Ga}_{25.7}\text{Ce}_{15.1}$  and  $\text{Au}_{60.3}\text{Ga}_{26.1}\text{Ce}_{13.6}$  near  $E_F$ . The black lines indicate the binding energy at which the spectral intensity starts to decrease. (b) Schematic image of a rigid-band-like shift in the Au-Ga-Ce ACs.

It should be pointed out that the energy difference between  $\Delta_{15.1}$  and  $\Delta_{13.6}$  is comparable to the slight shift of the main Au  $5d$  bands seen in the HAXPES spectra in Fig.4(b). In order to discuss the composition-ratio dependence, the number of valence electrons  $n_e$  is shown here. Note that the definition of  $n_e$  is the number of electrons which form the valence bands, *i.e.*, Au:  $5d^{10}, 6s^1$ , Ga:  $4s^2, 4p^1$ , and Ce:  $6s^2, 5d^1$ . The  $n_e$  for both composition ratio is calculated as follows:

$$\begin{aligned} \text{Au}_{59.2}\text{Ga}_{25.7}\text{Ce}_{15.1} : n_e \\ = 11 \times 0.592 + 3 \times 0.257 + 3 \times 0.151 = 7.74 \end{aligned} \quad (2)$$

$$\begin{aligned} \text{Au}_{60.3}\text{Ga}_{26.1}\text{Ce}_{13.6} : n_e \\ = 11 \times 0.603 + 3 \times 0.261 + 3 \times 0.136 = 7.82 \end{aligned} \quad (3)$$

From Equations (2) and (3),  $n_e$  of  $\text{Au}_{60.3}\text{Ga}_{26.1}\text{Ce}_{13.6}$  is larger than that of  $\text{Au}_{59.2}\text{Ga}_{25.7}\text{Ce}_{15.1}$ . When it is assumed that a rigid-band-like shift arises,  $E_F$  of  $\text{Au}_{60.3}\text{Ga}_{26.1}\text{Ce}_{13.6}$  is shifted to the unoccupied side relative to that of  $\text{Au}_{59.2}\text{Ga}_{25.7}\text{Ce}_{15.1}$ . Figure 5(b) shows the schematic image of such a rigid-band-like shift in Au-Ga-Ce ACs.  $\Delta_{13.6}$  should be larger than  $\Delta_{15.1}$  in the rigid-band-like shift when we consider the difference in  $n_e$  shown in Equations (2) and (3), which is consistent with the result of high-resolution PES. Moreover, the shift of Au  $5d$  bands in the valence-band HAXPES spectra is also explained by the rigid-band-like shift. Thus, the composition-ratio dependence found in the valence-band PES is explained by the rigid-band-like shift. Namely, the additional Ce injection into the tetrahedron (M7) sites hardly affects the substantial electronic structure for the Au-Ga-Ce ACs. From our study, we also conclude that the slight  $-\log T$ -like behavior in the resistivity of  $\text{Au}_{59.2}\text{Ga}_{25.7}\text{Ce}_{15.1}$ <sup>17)</sup> does not originate from the Kondo effect although the mechanisms are unclear at present.

#### 4. Summary

In summary, we have performed the HAXPES and high-resolution PES of AC  $\text{Au}_{59.2}\text{Ga}_{25.7}\text{Ce}_{15.1}$  and  $\text{Au}_{60.3}\text{Ga}_{26.1}\text{Ce}_{13.6}$ . The Ce  $4f$  states are found to be highly localized in both Au-Ga-Ce ACs. The overall electronic structure is mutually similar irrespective of the Ce injection in the tetrahedron sites. We have also observed the unexpected broadening in the  $3d^9 4f^1$  main peaks in the Ce  $3d$  core-level photoemission spectra of both Au-Ga-Ce ACs. From the comparison of the spectra of AC  $\text{Cd}_6\text{Ce}$ , we conclude that this broadening is caused by the effect of the disorders in the Au-Ga-Ce ACs. The composition-ratio (substitution-ratio) dependence of the electronic state is found as the rigid-band-like shift.

#### Acknowledgments

We acknowledge K. Nishimoto, Y. Arinaga, H. Hashizume, Y. Shimada, T. Usui, T. Miyazaki, Y. Chen, Y. Murakami, and N. Tanaka for supporting the HAXPES measurements. We also thank T. Morita for the support of the high-resolution PES measurements. The HAXPES measurements at SPring-8 BL19LXU were performed under the approval of RIKEN (Proposals Nos. 20200075, 20210068, and 20220071) at SPring-8. This work was financially supported by a Grant-in-Aid for Innovative Areas (JP19H05817, JP19H05818, JP20H05271, and JP22H04594), a Grant-in-Aid for Transformative Research (JP23H04867), a Grant-in-Aid for Scientific Research (JP19K14663, JP20K20900, JP22K03527, and JP24K03202) from JSPS and MEXT, and CREST (JP-MJCR2203) from JST. G. Nozue was supported by the Osaka university fellowship program of Super Hierarchical Materials Science Program and by the JSPS Research Fellowships for Young Scientists.

- 1) F. R. de Boer, J. C. P. Klaasse, P. A. Veenhuizen, A. Bohm, C. D. Bredl, U. Gottwick, H. M. Mayer, L. Pawlak, U. Rauschwalbe, H. Spille, and F. Steglich, *J. Magn. Magn. Mater.* **63**, 91 (1987).
- 2) M. J. Besnus, A. Essaihi, N. Hamdaoui, J. P. Kappler, A. Meyer, J. Pierre, P. Haen, and P. Lejay, *Physica B*, **171**, 350 (1991).
- 3) F. Steglich, J. Aarts, C. D. Bredl, W. Lieke, D. Meschede, W. Franz, and H. Schäfer, *Phys. Rev. Lett.* **43**, 1892 (1979).
- 4) F. M. Grosche, P. Agarwal, S. R. Julian, N. J. Wilson, R. K. W. Haselwimmer, S. J. S. Lister, N. D. Mathur, F. V. Carter, S. S. Saxena, and G. G. Lonzarich, *J. Phys.: Condens. Matter* **12**, L533 (2000).
- 5) K. Andres, J. E. Graebner, and H. R. Ott, *Phys. Rev. Lett.* **35**, 1779 (1975).
- 6) M. J. Besnus, J. P. Kappler, P. Lehmann, and A. Meyer, *Solid State Commun.* **55**, 779 (1985).
- 7) F. Steglich, U. Rauchschwalbe, U. Gottwick, H. M. Mayer, G. Sparn, N. Grewe, U. Poppe, and J. J. M. Franse, *J. Appl. Phys.* **57**, 3054 (1985).
- 8) J. D. Thompson, J. O. Willis, C. Godart, D. E. MacLaughlin, and L. C. Gupta, *Solid State Commun.* **56**, 169 (1985).
- 9) O. Trovarelli, C. Geibel, S. Mederle, C. Langhammer, F. M. Grosche, P. Gegenwat, M. Lang, G. Sparn, and F. Steglich, *Phys. Rev. Lett.* **85**, 626 (2000).
- 10) S. Nakatsuji, K. Kuga, Y. Machida, T. Tayama, T. Sakakibara, Y. Karaki, H. Ishimoto, S. Yonezawa, Y. Maeno, E. Pearson, G. G. Lonzarich, L. Balicas, H. Lee, and Z. Fisk, *Nat. Phys.* **4**, 603 (2008).
- 11) K. Deguchi, S. Matsukawa, N. K. Ssto, T. Hattori, K. Ishida, H. Takakura, and T. Ishimasa, *Nat. Mater.* **11**, 1013 (2012).
- 12) K. Deguchi, M. Nakayama, S. Matsukawa, K. Imura, K. Tanaka, T. Ishimasa, and N. K. Sato, *J. Phys. Soc. Jpn.* **84**, 023705 (2015).
- 13) R. Tamura, A. Ishikawa, S. Suzuki, T. Kotajima, Y. Tanaka, T. Seki, N. Shibata, T. Yamada, T. Fujii, C. W. Wang, M. Avdeev, K. Nawa, D. Okuyama, and T. Sato, *J. Am. Chem.* **143**, 19938 (2021).
- 14) K. Imura, K. Nobe, K. Deguchi, M. Matsunami, H. Miyazaki, A. Yasui, E. Ikenaga, and N. K. Sato, *J. Phys. Soc. Jpn.* **86**, 093702 (2017).
- 15) P. Boulet, M. C. de Weerd, M. Krnel, S. Vrtnik, Z. Jaglicic, and J. Delinsek, *Inorg. Chem.* **60**, 2526 (2021).
- 16) Y. Muro, T. Fukuhara, T. Namiki, T. Kuwai, A. Sakurai, A. Ishikawa, S. Suzuki, and R. Tamura, *Mater. Trans.* **62**, 321 (2021).
- 17) S. Suzuki, A. Motouri, K. Deguchi, T. Yamada, A. Ishikawa, T. Fujii, K. Nawa, T. J. Ssto, and R. Tamura, arXiv:2308.10070.
- 18) K. Momma and F. Izumi, *J. Appl. Crystallogr.* **44**, 1272 (2011).
- 19) K. Horiba, M. Taguchi, A. Chainani, Y. Takata, E. Ikenaga, D. Miwa, Y. Nishino, K. Tamasaku, M. Awaji, A. Takeuchi, M. Yabashi, H. Namagame, M. Taniguchi, H. Kumigashira, M. Oshima, M. Lippmaa, M. Kawasaki, H. Koinuma, K. Kobayashi, T. Ishikawa, and S. Shin, *Phys. Rev. Lett.* **93**, 236401 (2004).
- 20) A. Sekiyama, *J. Electron Spectrosc. Relat. Phenom.* **208**, 100 (2016).
- 21) M. Armbrüster and S. Lidin, *J. Alloys. Comd.* **307**, 141 (2000).
- 22) K. Nishimoto, R. Tamura, and S. Takeuchi, *Phys. Rev. B* **81**, 184201 (2010).
- 23) Z. M. Stadnik, D. Purdie, M. Garnier, Y. Baer, A. -P. Tsai, A. Inoue, K. Edagawa, and S. Takeuchi, *Phys. Rev. Lett.* **77**, 1777 (1996).
- 24) Z. M. Stadnik, D. Purdie, M. Garnier, Y. Baer, A. -P. Tsai, A. Inoue, K. Edagawa, S. Takeuchi, and K. H. J. Buschow, *Phys. Rev. B* **55**, 10938 (1997).
- 25) R. Tamura, Y. Murao, S. Takeuchi, T. Kiss, T. Yokoya, and S. Shin, *Phys. Rev. B* **65**, 224207 (2002).
- 26) H. Fujiwara, S. Naimen, A. Higashiya, Y. Kanai, H. Yomosa, K. Yamagami, T. Kiss, T. Kadono, S. Imada, A. Yamasaki, K. Takase, S. Otsuka, T. Shimizu, S. Shingubara, S. Suga, M. Yabashi, K. Tamasaku, T. Ishikawa, and A. Sekiyama, *J. Synchrotron Rad.* **23**, 735 (2016).
- 27) G. Funabashi, H. Fujiwara, A. Sekiyama, M. Hasumoto, T. Itoh, S. Kimura, P. Baltzer, and S. Suga, *Jpn. J. Appl. Phys.* **37**, 2265 (2008).
- 28) S. Suga, A. Sekiyama, G. Funabashi, J. Yamaguchi, M. Kimura, M. Tsujibayashi, T. Uyama, H. Sugiyama, Y. Tomida, G. Kuwahara, S. Kitayama, K. Fukushima, K. Kimura, T. Yokoi, K. Murakami, H. Fujiwara, Y. Saitoh, L. Plucinski and M. Schneider, *Rev. Sci. Instrum.* **81**, 105111 (2010).
- 29) M. Yano, A. Sekiyama, H. Fujiwara, Y. Amano, S. Imada, T. Muro, M. Yabashi, K. Tamasaku, A. Higashiya, T. Ishikawa, Y. Onuki, and S. Suga, *Phys. Rev. B* **77**, 035118 (2008).
- 30) J. C. Fuggle, F. U. Hillebrecht, Z. Zołnierek, R. Lässer, Ch. Feriburg, O. Gunnarsson, and K. Schönhammer, *Phys. Rev. B* **27**, 7330 (1983).
- 31) S. Imada and T. Jo, *J. Phys. Soc. Jpn.* **58**, 2665 (1989).
- 32) M. Sundermann, F. Strigari, T. Willers, J. Weinen, Y.F. Liao, K.-D. Tsuei, N. Hiraoka, H. Ishii, H. Yamaoka, J. Mizuki, Y. Zekko, E. D. Bauer, J. L. Sarrao, J. D. Thompson, P. Lejay, Y. Muro, K. Yutani, T. Takabatake, A. Tanaka, N. Hollmann, L. H. Tjeng, and A. Severing, *J. Electron Spectrosc. Relat. Phenom.* **209**, 1 (2016).
- 33) D. T. Adroja, S. K. Malik, B. D. Padalia, and R. Vijayaraghavan, *Solid State Commun.* **66**, 1201 (1988).
- 34) (Supplemental material) For details of the effects of polycrystalline structures, we have compared the Ce 3d core-level HAXPES spectra of the Au-Ga-Ce ACs with that of polycrystalline CePdSn.
- 35) S. Hüfner, *Photoelectron Spectroscopy* (Springer-Verlag, Berlin, 1995).
- 36) R. J. Cole, J. A. D. Matthew, and P. Weightman, *J. Electron Spectrosc. Relat. Phenom.* **72**, 255 (1995).
- 37) A. Sekiyama, J. Yamaguchi, A. Higashiya, M Obara, H. Sugiyama, M. Y. Kimura, S. Suga, S. Imada, I. A. Nekrasov, M. Yabashi, K. Tamasaku, and T. Ishikawa, *New J. Phys.* **12**, 043045 (2010).
- 38) M.B. Trzhaskovskaya, V. I. Nefedov and V. G. Yarzemesky, *At. Data Nucl. Data Tables*, **77**, 97 (2001).
- 39) M. B. Trzhaskovskaya, V. I. Nefedov and V. G. Yarzemesky, *At. Data Nucl. Data tables* **82**, 257 (2002).
- 40) M. B. Trzhaskovskaya, V. I. Nefedov and V. G. Yarzemesky, *At. Data Nucl. Data Tables*, **92**, 245 (2006).
- 41) M. B. Trzhaskovskaya and V. G. Yarzemesky, *At. Data Nucl. Data Tables*, **119**, 99 (2018).